ATLAS CONF Note

ATLAS-CONF-2017-079

December 11, 2017

Search for top squarks decaying to tau sleptons in pp collisions at $\sqrt{s} = 13$ TeV with the ATLAS detector

The ATLAS Collaboration

A search for direct pair production of top squarks in final states with two tau leptons, b-jets, and missing transverse momentum is presented, based on 36.1 fb^{-1} of proton–proton collision data recorded at $\sqrt{s} = 13$ TeV with the ATLAS detector at the Large Hadron Collider in 2015 and 2016. Two exclusive channels with either two hadronically decaying tau leptons or one hadronically and one leptonically decaying tau lepton are considered. No significant deviation from the Standard Model predictions is observed in the data. The analysis results are both interpreted in terms of model-independent limits and used to derive exclusion limits on the masses of the top squark $\tilde{t}_1$ and the tau slepton $\tilde{\tau}_1$ in a simplified model with a nearly-massless gravitino. In this model, masses up to $m(\tilde{t}_1) = 1.16$ TeV and $m(\tilde{\tau}_1) = 1.00$ TeV are excluded at 95 % confidence level.

ATLAS-CONF-2017-079
14 December 2017

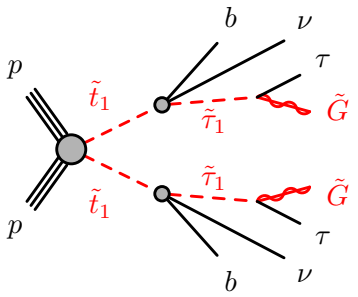

FIG. 1. The simplified model for production and decay of supersymmetric particles considered in this analysis. The branching ratios are assumed to be 100 % in the decay mode shown, both for the decay of the top squark as well as for the decay of the tau slepton. All sparticles not appearing in this diagram are assumed to be too massive to be relevant for LHC phenomenology. The top squark decay vertex is drawn as a blob to indicate that the three-body decay is assumed to happen through an off-shell chargino.

1 Introduction

Supersymmetry (SUSY) [1–6] (see Ref. [7] for a review) extends the Standard Model (SM) with an additional symmetry that connects bosons and fermions, thereby providing answers to several of the open questions in the SM. It predicts the existence of new particles that have the same mass and quantum numbers as their SM partners but differ in spin by one half-unit. Since no such particles have been observed as of today, SUSY, if realized in nature, must be a broken symmetry, allowing the supersymmetric partner particles to have higher masses than their SM counterparts. In the model considered in this work, the conservation of R-parity is assumed [8], so that the supersymmetric particles (sparticles) are produced in pairs, and the lightest supersymmetric particle (LSP) is stable, providing a viable candidate for dark matter.

This note describes a search for SUSY in a benchmark scenario motivated by gauge-mediated SUSY breaking (GMSB) [9–11] and natural gauge mediation (nGM) [12]. In this scenario, only three sparticles are assumed to be sufficiently light to be relevant in collider phenomenology: the lightest scalar top quark partner (top squark, $\tilde{t}_1$) the lightest scalar tau lepton partner (tau slepton, $\tilde{\tau}_1$), and a nearly massless gravitino $\tilde{G}$ ($m(\tilde{G}) < 1\,\text{GeV}$).

The search strategy is optimized using a simplified model [13, 14] with this limited sparticle content. The relevant parameters are the sfermion masses $m(\tilde{t}_1)$ and $m(\tilde{\tau}_1)$. The process is illustrated in Fig. 1. The top squark is assumed to be light [15, 16] and directly pair-produced through the strong interaction. Each top squark decays into a b-quark, a tau neutrino, and a tau slepton which in turn decays into a tau lepton and a gravitino. The branching ratios are set to 100 %, and the $\tilde{\tau}_1$ decay is assumed to be prompt. As the tau-slepton mixing is not relevant for this analysis, the tau-slepton mixing matrix is chosen such that the tau slepton is an equal mix of the superpartners of the left- and the right-chiral tau lepton. An alternative scenario with a neutralino $\tilde{\chi}_1^0$ as LSP, which would suggest a high branching ratio of direct decays $\tilde{t}_1 \to t\tilde{\chi}_1^0$, has been studied elsewhere [17–21].

The search uses proton–proton (pp) collision data collected with the ATLAS detector at $\sqrt{s} = 13\,\text{TeV}$ in 2015 and 2016, with a combined integrated luminosity of $36.1\,\text{fb}^{-1}$. A previous analysis considering the same three-body decay mode of the top squark to the tau slepton based on $20\,\text{fb}^{-1}$ of ATLAS data at $\sqrt{s} = 8\,\text{TeV}$ has set lower limits on the mass of the top squark $\tilde{t}_1$ of up to 650 GeV [22]. The combined

LEP lower limit on the mass of the tau slepton, derived from searches for $\tilde{\tau} \rightarrow \tau\tilde{\chi}_1^0$ decays, ranges between 87 and 96 GeV depending on the assumed mass of the lightest neutralino [23]. Models with small mass differences between the tau slepton and the lightest neutralino of up to approximately 10 GeV are not excluded by the LEP experiments. For a branching ratio $\tilde{\tau} \rightarrow \tau\tilde{\chi}_1^0$ of 100 % and a massless $\tilde{\chi}_1^0$, the lower limit on the tau slepton mass is around 90 GeV. The limits obtained from models with direct production of tau sleptons published by the LHC experiments [24–26] are not more stringent than those provided by LEP.

Depending on the decay modes of the tau leptons, final states with two tau leptons can be classified into one of the following three channels. Events with both tau leptons decaying hadronically belong to the had-had channel. The lep-had channel refers to events in which one of the tau leptons decays leptonically and the other hadronically. Final states where both tau leptons decay leptonically have the smallest branching fraction and are not considered, as studies showed that they would not contribute significantly to the sensitivity of the analysis.

This note is structured as follows: Sec. 2 gives a brief description of the ATLAS detector. Section 3 defines the recorded and simulated events used in the analysis, while Sec. 4 summarizes the reconstruction of physics objects such as leptons and jets and the kinematic variables used in the event selection. In Sec. 5, the selection to obtain a signal-enriched event sample is described. The background determination is described in Sec. 6, followed by a discussion of the methods used to derive the corresponding systematic uncertainties in Sec. 7. Section 8 presents the analysis results and their interpretation. The note concludes with a brief summary in Sec. 9.

2 ATLAS Detector

The ATLAS detector [27] is a multi-purpose particle detector with a forward–backward symmetric cylindrical geometry and nearly 4π coverage in solid angle.[1] It consists of, starting from the interaction point and going outwards, an inner tracking detector, electromagnetic and hadronic calorimeters, and a muon spectrometer. The inner tracking detector covers the pseudorapidity range $|\eta| < 2.5$ and consists of silicon pixel, silicon microstrip, and transition radiation detectors, immersed in a 2 T axial magnetic field provided by a thin superconducting solenoid. The insertable B-layer, the innermost layer of the silicon pixel detector, was added before the $\sqrt{s} = 13$ TeV data-taking and provides high-resolution hits to improve the tracking and b-tagging performance [28]. The calorimeter system covers pseudorapidities up to $|\eta| < 4.9$. Electromagnetic energy measurements with high granularity are provided by lead/liquid-argon sampling calorimeters in the region $|\eta| < 3.2$, and a sampling calorimeter with scintillator tiles and steel absorbers is used for hadronic calorimetry within $|\eta| < 1.7$. The forward regions are instrumented with sampling calorimeters using liquid-argon as active medium for both the electromagnetic and hadronic calorimetry. The muon spectrometer features three large superconducting toroid magnets with eight coils each, precision-tracking detectors in the region $|\eta| < 2.7$, and fast, dedicated chambers for triggering in the region $|\eta| < 2.4$. Collision events are selected for recording by a two-stage trigger system, which has been upgraded for the run at $\sqrt{s} = 13$ TeV [29]. It consists of a hardware-based trigger as the first level,

[1] ATLAS uses a right-handed coordinate system with its origin at the nominal interaction point (IP) in the center of the detector and the z-axis along the beam pipe. The x-axis points from the IP to the center of the LHC ring, and the y-axis points upward. Cylindrical coordinates (r, ϕ) are used in the transverse plane, ϕ being the azimuthal angle around the z-axis. The pseudorapidity is defined in terms of the polar angle θ as $\eta = -\ln\tan(\theta/2)$. When the mass of a particle cannot be neglected, the rapidity $y = 0.5 \ln\left[(E + p_z)/(E - p_z)\right]$ is used instead of the pseudorapidity η to specify its direction.

TABLE I. Overview of the simulation codes, parton distribution function sets and parameters used to simulate the Standard Model background processes and the supersymmetric signal process. Corresponding references are given in the text.

Process	Matrix element	PDF set	Parton shower	PDF set	Tune
$t\bar{t}$	Powheg-Box v2	CT10	Pythia 6.428	CTEQ6L1	Perugia 2012
single top	Powheg-Box v1	CT10	Pythia 6.428	CTEQ6L1	Perugia 2012
$t\bar{t}H$	aMC@NLO 2.2.2	CT10	Herwig++ 2.7.1	CTEQ6L1	UE-EE-5
$t\bar{t}V$	aMC@NLO 2.3.3	NNPDF3.0 NLO	Pythia 8.210	NNPDF2.3 LO	A14
tWZ	aMC@NLO 2.3.2	NNPDF3.0 NLO	Pythia 8.210	NNPDF2.3 LO	A14
tZ	MadGraph5 2.2.1	CTEQ6L1	Pythia 6.428	CTEQ6L1	Perugia 2012
multi-top	MadGraph5 2.2.2	NNPDF2.3 LO	Pythia 8.186	NNPDF2.3 LO	A14
V + jets	Sherpa 2.2.1	NNPDF3.0 NNLO			
VV (1)	Sherpa 2.2.1	NNPDF3.0 NNLO			
VV (2)	Sherpa 2.1.1	CT10			
VVV	Sherpa 2.2.2	NNPDF3.0 NNLO			
SUSY	MadGraph5 2.2.3 and 2.3.3	NNPDF2.3 LO	Pythia 8.186, 8.205 or 8.210	NNPDF2.3 LO	A14

followed by the software-based high-level trigger, which is able to run reconstruction and calibration algorithms similar to those used offline, reducing the event rate to about 1 kHz.

3 Dataset and Simulation

The dataset analyzed in this note was recorded with the ATLAS detector from pp collisions delivered by the Large Hadron Collider at CERN in 2015 and 2016 at a center-of-mass energy of $\sqrt{s} = 13$ TeV [30]. Collision events are selected with triggers on electrons or muons (lep-had) and $E_{\mathrm{T}}^{\mathrm{miss}}$ or two hadronic tau leptons (had-had). The total integrated luminosity of the dataset after the application of data-quality requirements that ensure that all subdetectors are functioning normally is 36.1 fb^{-1} with an uncertainty of 3.2 %. The uncertainty was derived, following a methodology similar to that detailed in Ref. [31], from a preliminary calibration of the luminosity scale using x–y beam-separation scans performed in August 2015 and May 2016.

Monte Carlo (MC) simulation is used to generate samples of collision events, which model the expected kinematics of the supersymmetric signal models and allow the prediction of the contributions of the various SM background processes. The MC generators, parton distribution function sets and parameters used to simulate the Standard Model background processes and the supersymmetric signal process of the simplified model are summarized in Table I. Additional MC samples are used to estimate systematic uncertainties, as described in Sec. 7, and for the major background processes, data-driven methods are used to augment the accuracy of the MC-based estimates (cf. Sec. 6).

Signal samples were generated from leading-order matrix elements (ME) with MadGraph5 v2.2.3 and v2.3.3 [32] interfaced to Pythia 8.186, 8.205 or 8.210 [33, 34] with the ATLAS 2014 (A14) [35] set of tuned parameters (tune) for the modeling of the parton showering (PS), hadronization and underlying event. The matrix element calculation was performed at tree-level and includes the emission of up to two

additional partons. The parton distribution function (PDF) set used for the generation was NNPDF2.3 LO [36]. The ME–PS matching was done using the CKKW-L [37] prescription, with the matching scale set to one quarter of the top squark mass. Signal cross sections were calculated to next-to-leading order in the strong coupling constant, adding the resummation of soft gluon emission at next-to-leading-logarithmic accuracy (NLO+NLL) [38–40].

Production of top-quark pairs and of single top quarks in the s- and t-channel or associated with W bosons was simulated with Powheg-Box v2 [41] interfaced to Pythia 6.428 [42] for the parton shower, hadronization, and underlying event, using the CT10 set [43] of parton distribution functions in the matrix element calculations and the CTEQ6L1 PDF set [44] with the Perugia 2012 tune [45] for the shower and underlying event. Associated production of top-quark pairs and Higgs bosons was simulated with aMC@NLO [32] interfaced to Herwig++ 2 [46, 47], using the UE-EE-5 tune [48]. For $t\bar{t}+V$, where V is a W or Z boson, and tWZ production, aMC@NLO with the NNPDF3.0 NLO PDF set [49] and Pythia 8.210 [34] were used. Finally, production of tZ and three or four top quarks (multi-top) was simulated with MadGraph5 and Pythia. The EvtGen program [50] was used for all samples with top quarks and the signal samples to model the properties of the bottom and charm hadron decays.

Drell-Yan production of charged and uncharged leptons, $Z/\gamma^* \to \ell^+\ell^-$ and $Z \to \nu\bar{\nu}$, and leptonic decays of W bosons, $W \to \ell\nu$, in association with jets (V + jets) were simulated with Sherpa [51], using the Sherpa parton shower [52] and a dedicated tuning developed by the Sherpa authors. Sherpa was also used for the simulation of diboson production (VV) and leptonic decays of triboson production (VVV). The diboson samples include one set of tree-induced processes with dileptonic and semileptonic decays, VV (1), and a second set with electroweak $VVjj$ production and loop-induced production with leptonic decays, VV (2).

All simulated background events were passed through a full Geant4 [53] simulation of the ATLAS detector [54]. For signal events, a fast detector simulation was used, which is based on a parameterization of the performance of the electromagnetic and hadronic calorimeters [55] and on Geant4 for all other detector components. The same algorithms were used for the reconstruction of physics objects in simulated signal and background events and in collision data. The agreement between simulated events and collision data is improved by weighting the simulated events to account for differences in the lepton-trigger efficiencies, lepton reconstruction, identification and isolation efficiencies, b-tagging, and jet-vertex-tagging efficiencies using correction factors derived in dedicated studies.

The effect of additional pp interactions in the same and nearby bunch crossings ("pile-up") was taken into account by overlaying the hard-scattering process with soft pp interactions generated with Pythia 8.186 using the A2 tune [56] and the MSTW2008LO PDF set [57]. Simulated events were reweighted to make the distribution of the average number of simultaneous pp collisions match that of the recorded dataset.

4 Event Reconstruction

The data recorded in collision events are processed to reconstruct and identify physics objects needed for the event selection, and to reject events of insufficient quality. Candidate events are required to have a reconstructed vertex [58] with at least two associated tracks with a transverse momentum $p_{\mathrm{T}} > 400\,\mathrm{MeV}$. If there are several such vertices, the one with the largest scalar sum of p_{T}^2 of its associated tracks is used as the primary collision vertex.

Jets are reconstructed from topological energy clusters in the calorimeters [59] using the anti-k_t algorithm [60] with radius parameter $R = 0.4$ and are calibrated to the hadronic scale, accounting for the impact of pile-up in the event. The calibration is improved with the global sequential correction scheme [61]. Jets with $p_{\mathrm{T}} > 20\,\mathrm{GeV}$ and $|\eta| < 2.8$ are retained. In addition, jets need to fulfill basic quality criteria; an event is discarded if any selected jet does not meet these criteria [62]. Pile-up is suppressed further by rejecting jets with $p_{\mathrm{T}} < 60\,\mathrm{GeV}$ and $|\eta| < 2.4$ if their origin is found not to be compatible with the primary vertex based on the output of a jet-vertex-tagging algorithm [63].

A multivariate discriminant based on track impact parameters and reconstructed secondary vertices [64, 65] is employed to identify jets originating from b-hadron decays with $|\eta| < 2.5$. The chosen working point has a b-tagging efficiency of 77 % and rejection factors of 134, 6, and 22, for light-quark and gluon jets, c-quark jets, and hadronically decaying tau leptons, τ_h, respectively, as evaluated on a simulated sample of $t\bar{t}$ events.

To reconstruct τ_h candidates and associate them to a primary vertex, a dedicated algorithm is used that is seeded from jets reconstructed with the anti-k_t algorithm with a radius parameter $R = 0.4$ and fulfilling $p_{\mathrm{T}} > 10\,\mathrm{GeV}$ and $|\eta| < 2.5$ [66]. Only the visible part of the τ_h decay is reconstructed. An energy calibration derived independently of the jet energy scale is applied to the reconstructed τ_h [67]. The analysis uses τ_h candidates with $p_{\mathrm{T}} > 20\,\mathrm{GeV}$ and $|\eta| < 2.5$, excluding the calorimeter transition region $1.37 < |\eta| < 1.52$ because of its larger uncertainty in jet direction measurements, and requires the presence of 1 or 3 associated tracks (prongs) and a total track charge of ± 1. A boosted decision tree discriminant is used to reject jets that do not originate from a hadronically decaying tau lepton, with a working point yielding a combined tau reconstruction and identification efficiency of 55 % (40 %) for 1-prong (3-prong) τ_h [68]. For the background estimate using the fake-factor method, which is described in Sec. 6.1, a looser set of identification criteria, called "AntiID", are used.

For electrons and muons, two sets of identification criteria are defined: the *baseline* definitions are used for lepton vetoes and the overlap removal procedure described below, while *signal* definitions are used when event selections require the presence of a lepton.

Electron candidates are reconstructed from clusters in the electromagnetic calorimeter matched to tracks in the inner tracking detector. Baseline electrons must satisfy a loose likelihood-based identification [69, 70] and have $|\eta_{\mathrm{cluster}}| < 2.47$ and $p_{\mathrm{T}} > 10\,\mathrm{GeV}$. Signal electrons must have $p_{\mathrm{T}} > 25\,\mathrm{GeV}$ and satisfy the tight likelihood-based quality criteria. In addition, they must fulfill requirements on the track and calorimetric isolation, the transverse impact parameter significance ($|d_0| / \sigma(d_0) < 5$) and the longitudinal impact parameter ($|z_0 \sin(\theta)| < 0.5\,\mathrm{mm}$).

The muon reconstruction combines tracks recorded in the muon system and the inner tracking detector. Baseline muons must have $p_{\mathrm{T}} > 10\,\mathrm{GeV}$ and $|\eta| < 2.7$ and fulfill medium quality criteria [71]. Signal muons must further be isolated and satisfy $p_{\mathrm{T}} > 25\,\mathrm{GeV}$ and $|\eta| < 2.5$ as well as requirements on the track impact parameters ($|d_0| / \sigma(d_0) < 3$ and $|z_0 \sin(\theta)| < 0.5\,\mathrm{mm}$).

The object reconstruction algorithms described above work independently from each other and may therefore assign the same detector signature to multiple objects. A sequence of geometrical prescriptions are applied to resolve ambiguities by removing objects. In particular, tau candidates near electrons or muons ($\Delta R_y = \sqrt{\Delta\phi^2 + \Delta y^2} < 0.2$) are discarded as part of this procedure. No jet is allowed near an electron or a muon: for $\Delta R_y < 0.2$, the jet is removed, while for $0.2 < \Delta R_y < 0.4$, the lepton is removed instead.

The missing transverse momentum $\vec{p}_{\mathrm{T}}^{\,\mathrm{miss}}$ is defined as the negative vector sum of the transverse momenta of all identified physics objects (electrons, photons, muons, tau leptons, jets) and an additional soft term.

The soft term is constructed from all tracks that are not associated with any reconstructed physics object but associated to the identified primary collision vertex [72, 73]. In this way, the missing transverse momentum is adjusted for the best calibration of the jets and the other identified physics objects above, while maintaining pileup independence for the soft term. Frequently, only the magnitude $E_{\mathrm{T}}^{\mathrm{miss}} \equiv |\vec{p}_{\mathrm{T}}^{\,\mathrm{miss}}|$ is used.

4.1 Analysis Variables

Besides basic kinematic quantities, the variables described below are used in the event selections.

The transverse mass m_{T} is computed as the invariant mass of a lepton ℓ and the missing momentum in the event projected onto the transverse plane:

$$m_{\mathrm{T}} = \sqrt{2\, E_{\mathrm{T}}^{\mathrm{miss}}\, p_{\mathrm{T},\ell} \cdot \left(1 - \cos\left(\Delta\phi\left(\vec{p}_{\mathrm{T}}^{\,\mathrm{miss}}, \vec{p}_{\mathrm{T},\ell}\right)\right)\right)}, \tag{1}$$

where $p_{\mathrm{T},\ell}$ is the lepton's transverse momentum. In W+jets events, the m_{T} distribution will have a cut-off around the W-boson mass.

The stransverse mass m_{T2} [74–76] is employed in this analysis foremost to target the top pair background. It is a generalization of the transverse mass for final states with two invisible particles. It assumes two identical particles that decay into one visible and one invisible product each, and provides an upper bound on the mother particle's mass. This is achieved by considering all possible ways to distribute the measured $\vec{p}_{\mathrm{T}}^{\,\mathrm{miss}}$ between the invisible particles of the assumed decay.

In di-leptonic events, m_{T2} is constructed using the leptons as the visible particles. The $\vec{p}_{\mathrm{T}}^{\,\mathrm{miss}}$ is assumed to stem from a pair of neutrinos. The resulting variable is a powerful discriminant against background events with top-antitop or WW production, as it is bounded from above by m_W for these, while signal events do not respect this bound.

Furthermore, the invariant mass $m(\ell_1, \ell_2)$ of the two reconstructed leptons (including τ_h), as well as H_{T}, defined as the scalar sum of the p_{T} of the two leading jets, are used.

5 Event Selection

Several event selections (regions) are defined for the lep-had and had-had channels, starting from similar preselections that differ only in the choice of event triggers and the required numbers of reconstructed tau leptons and light leptons, i.e. electrons and muons. Prompt light leptons are not distinguished from light leptons originating from decays of tau leptons. Therefore, in the background estimates, processes with prompt light leptons contribute in the same way as processes with leptonic decays of tau leptons. The event selections for the two channels are mutually exclusive. They can therefore be statistically combined in the interpretation of the results.

TABLE II. Comparison of the preselections in the lep-had and had-had channel. The leading (subleading) objects are referred to using indices, e. g. jet_1 (jet_2).

Preselection	lep-had	had-had
Trigger	single-electron or single-muon trigger	$E_{\text{T}}^{\text{miss}}$ or di-tau trigger
Leptons	exactly one τ_h + one signal electron or muon no additional baseline electron or muon or τ_h	exactly two τ_h no baseline electron or muon
Trigger-related requirements	$p_{\text{T}}(e,\mu) > 27\,\text{GeV}$	$E_{\text{T}}^{\text{miss}} > 180\,\text{GeV}$ or $p_{\text{T}}(\tau_{1,2},\text{jet}_1) > 50, 40, 80\,\text{GeV}$
$p_{\text{T}}(\text{jet}_2)$	$> 26\,\text{GeV}$	$> 20\,\text{GeV}$
$p_{\text{T}}(\tau)$	$> 70\,\text{GeV}$	$> 70\,\text{GeV}$
$n_{b\text{-jet}}$	≥ 1	≥ 1

5.1 Preselection

The preselection requirements for the two channels are summarized in Table II. In the lep-had channel, events selected by single-electron or single-muon triggers are used. The had-had channel uses a logical OR of an $E_{\text{T}}^{\text{miss}}$ trigger and a combined trigger selecting events with two tau leptons and one additional jet at the first trigger level. The preselection adds suitable requirements to avoid working in the turn-on regime of the trigger efficiency. For events selected by the single-lepton triggers, the p_{T} of the light lepton is required to be at least 27 GeV. For the $E_{\text{T}}^{\text{miss}}$ trigger, $E_{\text{T}}^{\text{miss}}$ needs to exceed 180 GeV, and for the combined trigger, the requirements are at least 50 GeV (40 GeV) for the p_{T} of the leading (sub-leading) τ_h, and $p_{\text{T}} > 80$ GeV for the leading jet. The trigger efficiencies, from which the scale factors are computed that correct for small differences between simulation and collision data, are measured as a function of the lepton properties reconstructed offline, therefore these are matched to the leptons reconstructed in the trigger.

All candidate events must have at least two jets with p_{T} larger than 26 GeV (20 GeV) in the lep-had (had-had) channel. For the lep-had channel, the preselection requires exactly one τ_h, exactly one signal electron or muon, and no further baseline leptons. For the had-had channel, exactly two τ_h are required, and no baseline light leptons must be present. No requirement on the electric charge of the leptons is applied in the preselection, as both events with opposite-charge and events with same-charge lepton pairs are used in this analysis. In addition, in all regions of both the lep-had and had-had channels, the leading tau lepton must have $p_{\text{T}} > 70$ GeV and events are required to have at least one b-tagged jet.

5.2 Signal Selections

Two signal regions (SRs) are defined, one for the lep-had channel and one for the had-had channel. Both SR selections are based on the preselection described above, where in addition the lepton pair has to have opposite electric charge, as same-charge lepton pairs are not predicted by the signal model. They have been optimized to give the largest sensitivity to the targeted signal model in terms of the discovery p-value computed using a ratio of Poisson means [77, 78].

The variables with the best discrimination power between signal and background are the missing transverse momentum and stransverse mass. The optimal selection thresholds on these two variables are different in the two channels. In the lep-had (had-had) channel, the signal selection requires $m_{\text{T2}} > 100$ GeV

(80 GeV) and $E_{\mathrm{T}}^{\mathrm{miss}} > 230$ GeV (200 GeV), the lep-had selection needing slightly higher thresholds to achieve the same discrimination power between signal and background. A summary of the SR definitions is included in the last column of Tables III and IV for the lep-had and had-had channels, respectively.

6 Background Estimation

The general strategy for estimating the SM background in this analysis is to develop dedicated control regions (CRs) for the most important background contributions. These CRs provide data-driven constraints on the overall normalization of the respective background processes, whereas the shape of the kinematic distributions is taken from simulation. A maximum-likelihood fit is performed for all control-region yields simultaneously in order to obtain the normalization factors. The normalization factors from this background fit are then extrapolated using simulation to obtain the expected yields in the signal region. Therefore, all control-region selections must be mutually exclusive, with respect to each other as well as to the signal regions. The correctness of the extrapolation is checked in additional selections called validation regions (VRs), which cover the intermediate range in m_{T2} between the control and the signal regions, without overlapping either.

The targeted final state has two tau leptons, two b-quarks and missing transverse momentum. The dominant SM background process with this signature is pair production of top quarks. This background process can contribute in two different ways. In the first case, the objects from the top-quark decays are correctly reconstructed. One of the W bosons from the top-quark decays yields a hadronically decaying tau lepton; the other W boson decays into a light lepton in the lep-had channel, either directly or through a tau-lepton decay, or into a second hadronically decaying tau lepton in the had-had channel. In the second case, the background events contain a fake tau lepton, i.e. objects which are not a tau lepton, most often a jet or an electron, but reconstructed as a hadronically decaying tau lepton. The probability of falsely identifying a jet or an electron as a tau lepton is only on the order of a few percent, but on the other hand, the branching ratio of W bosons into jets or electrons is larger than that into hadronically decaying tau leptons. Moreover, the requirement on m_{T2} is more efficient at rejecting $t\bar{t}$ events with real tau leptons. Therefore, $t\bar{t}$ events with fake tau leptons dominate after applying the signal region selections. As the nature and quality of the modeling in simulation of these two background components from $t\bar{t}$ events may be very different, they are treated as separate background components in the following. The CRs and methods to estimate the background from $t\bar{t}$ events are introduced in Sections 6.1 and 6.2.

Sub-dominant contributions to the SM background come from diboson production, where often a jet is falsely identified to originate from a b-hadron decay, or $t\bar{t}$ production in association with a vector boson, where mostly the additional vector boson is a Z boson that decays to neutrinos. The CRs for these background processes are based on a selection of events with light leptons rather than hadronically decaying tau leptons, in order to achieve good purity and sufficiently high statistics in the CRs. A common normalization factor for the lep-had and had-had channels is derived. These CRs are defined in Sec. 6.3.

Finally, smaller contributions come from vector-boson production (W+jets and Z+jets, collectively denoted as V+jets) and single top production. Multi-top, triboson production, and $t\bar{t}$ production in association with a Higgs boson contribute very little to the signal regions and are therefore summarized under the label "others" in the following. The contributions for all of these are estimated directly from simulation and normalized to the generator cross section for triboson production [79] and multi-top production, and higher-order cross-section calculations for V+jets, $t\bar{t}H$ and single top production [80–86]. Contributions

from multi-jet events are not relevant for the analysis, as has been verified using data-driven methods. The multi-jet background is therefore neglected.

One signal benchmark point has been chosen to illustrate the behavior of the signal in comparison to the background processes in kinematic distributions. The mass parameters for this benchmark point are $m(\tilde{t}_1) = 1100\,\text{GeV}$ and $m(\tilde{\tau}_1) = 590\,\text{GeV}$. A larger mass splitting between the top squark and the tau slepton yields more energetic b-tagged jets in the final state, whereas a higher tau-slepton mass yields tau leptons with higher transverse momentum. As both the top squark and the tau slepton have invisible particles among their decay products, the $E_{\text{T}}^{\text{miss}}$ spectrum does not depend strongly on the mass of the intermediate particle, the tau slepton.

6.1 Lep-Had Channel

TABLE III. Definitions of the $t\bar{t}$ control and validation regions and the signal region in the lep-had channel. A dash means that no requirement on this variable is applied. The brackets indicate a range that the variable is required to lie in. A common preselection as given in Table II for the lep-had channel is applied.

Variable	CR LH $t\bar{t}$-real	VR LH $t\bar{t}$-real	VR LH $t\bar{t}$-fake (OS)	VR LH $t\bar{t}$-fake (SS)	SR LH
charge(ℓ,τ)	opposite	opposite	opposite	same	opposite
$m_{\text{T2}}(\ell,\tau)$	$< 60\,\text{GeV}$	[60, 100] GeV	[60, 100] GeV	$> 60\,\text{GeV}$	$> 100\,\text{GeV}$
$E_{\text{T}}^{\text{miss}}$	$> 210\,\text{GeV}$	$> 210\,\text{GeV}$	$> 150\,\text{GeV}$	$> 150\,\text{GeV}$	$> 230\,\text{GeV}$
$m_{\text{T}}(\ell)$	$> 100\,\text{GeV}$	$> 100\,\text{GeV}$	$< 100\,\text{GeV}$	—	—
$m(\ell,\tau)$	—	—	$> 60\,\text{GeV}$	—	—

The contribution of background events with real hadronically decaying tau leptons in the lep-had channel is estimated from simulation. For top-quark pair production in particular, only the shape of the distribution of the observables is taken from simulation but the overall normalization is derived from a dedicated CR. For events with fake tau leptons, it is difficult to design a CR with sufficiently high event yields and purity. Moreover, the estimate for this background from simulation does not agree with the observed data in the VRs. Therefore, the background estimate for events with fake tau leptons is derived using a data-driven method called the fake-factor method discussed below.

The CR and three VRs enriched in top-quark events or events with fake tau leptons are defined in Table III. As explained above, the CR and VRs cover a lower m_{T2} range, with the VRs located between the CR and the SR to check the extrapolation in this variable. In all of these regions, the preselection requirements for the lep-had channel from Table II are applied.

In the opposite-sign regions, the transverse mass $m_{\text{T}}(\ell)$ of the light lepton and the missing transverse momentum is used to separate $t\bar{t}$ events with real tau leptons from those with fakes. Events with top-quark pairs, where one of the top quarks decays to a light lepton and the other decays hadronically, and a jet from the hadronic W-boson decay is misidentified as the tau lepton, yield mostly small values of m_{T}. In these events, there is only one neutrino (from the leptonic W-boson decay), so the transverse mass has an endpoint around the W-boson mass. Events where both the light lepton and the hadronically decaying tau lepton are real involve more neutrinos, leading to tails of the m_{T} distribution that go beyond this endpoint. The extrapolation from the control region to the signal region is done in m_{T2}, which is correlated with m_{T}, but the validation regions cover the full m_{T} range so that any potential bias from the correlation of m_{T} and m_{T2} would be visible there.

As the purity of VR LH $t\bar{t}$-fake (OS) in $t\bar{t}$ events with fake tau leptons is low, an additional validation region, VR LH $t\bar{t}$-fake (SS), with a same-sign requirement is defined. The same-sign requirement is very efficient at rejecting events where both tau leptons are real and originate from the W bosons in a $t\bar{t}$ event. For jets misidentified as tau leptons, the correlation between their charge and the charge of the light lepton in $t\bar{t}$ events is much smaller; thus, events with fake tau leptons are more likely to pass the same-sign selection.

Distributions of the main discriminating variables $m_{\mathrm{T2}}(\ell,\tau)$ and $E_{\mathrm{T}}^{\mathrm{miss}}$ in the CR and the three VRs of the lep-had channel are shown in Fig. 2. For $t\bar{t}$ production with real tau leptons, $t\bar{t}+V$ and diboson production, the normalization obtained from the background fit (cf. Table VIII) is used. For single-top production and V + jets, the theory prediction for the cross section is used. All contributions from events with fake tau leptons (labeled "fake τ + e/μ" in the legend) are estimated using the fake-factor method. All other processes, which are expected to give only small contributions, are merged into one histogram ("others"). All selection requirements are applied in all plots, with the exception of the upper left plot, where the requirement on $m_{\mathrm{T2}}(\ell,\tau)$ is not applied, but indicated by a vertical line instead. The agreement between the predicted Standard Model background and the observed data is good. The largest differences are found in the top left plot at $m_{\mathrm{T2}}(\ell,\tau) = 70\,\mathrm{GeV}$ and in the first bin in the top right plot of $E_{\mathrm{T}}^{\mathrm{miss}}$. They correspond to the small excess in VR LH $t\bar{t}$-real.

Fake-Factor Method

The fake-factor method is used to estimate the contribution of events in the lep-had channel in which the reconstructed tau lepton is a fake. This estimate is obtained as the product of the number of events passing a selection where the requirements on the tau identification are loosened and the fake factor, which relates the numbers of events with looser tau-lepton candidates and events where tau leptons pass the nominal identification criteria.

To compute the fake factor, a looser set of criteria for the tau identification is used ("AntiID"), which is orthogonal to the default working point used in the analysis ("ID"), cf. Sec. 4. The value FF is the ratio of the numbers of events with ID and AntiID tau leptons in the measurement region (MR) in data, $N^{\star}(\mathrm{data,\,MR})$, where $\star$ is ID or AntiID. It depends on the p_{T} and the number of associated tracks of the tau lepton candidate. No strong dependence on the pseudorapidity has been observed. The contamination from events with real tau leptons $N^{\star}_{\mathrm{real}}(\mathrm{MC,\,MR})$ is estimated from simulation and subtracted when taking the ratio,

$$FF = \frac{N^{\mathrm{ID}}(\mathrm{data,\,MR}) - N^{\mathrm{ID}}_{\mathrm{real}}(\mathrm{MC,\,MR})}{N^{\mathrm{AntiID}}(\mathrm{data,\,MR}) - N^{\mathrm{AntiID}}_{\mathrm{real}}(\mathrm{MC,\,MR})}.$$

The measurement region is chosen such that this contamination is as small as possible. It is about 1 % for AntiID and about 10 % for ID tau leptons. The number of events with fake tau leptons passing the target selection (TR) is then estimated as

$$N_{\mathrm{fakes}}(\mathrm{TR}) = \left(N^{\mathrm{AntiID}}(\mathrm{data,\,TR}) - N^{\mathrm{AntiID}}_{\mathrm{real}}(\mathrm{MC,\,TR})\right) \cdot FF,$$

where again $N^{\mathrm{AntiID}}_{\mathrm{real}}(\mathrm{MC,\,TR})$ is a correction which accounts for the contamination from events with real tau leptons and is estimated using simulation.

Both the number of events with looser tau identification in the target selection as well as the fake factor can be obtained from data. The only input taken from simulation are small corrections that account for events with real tau leptons.

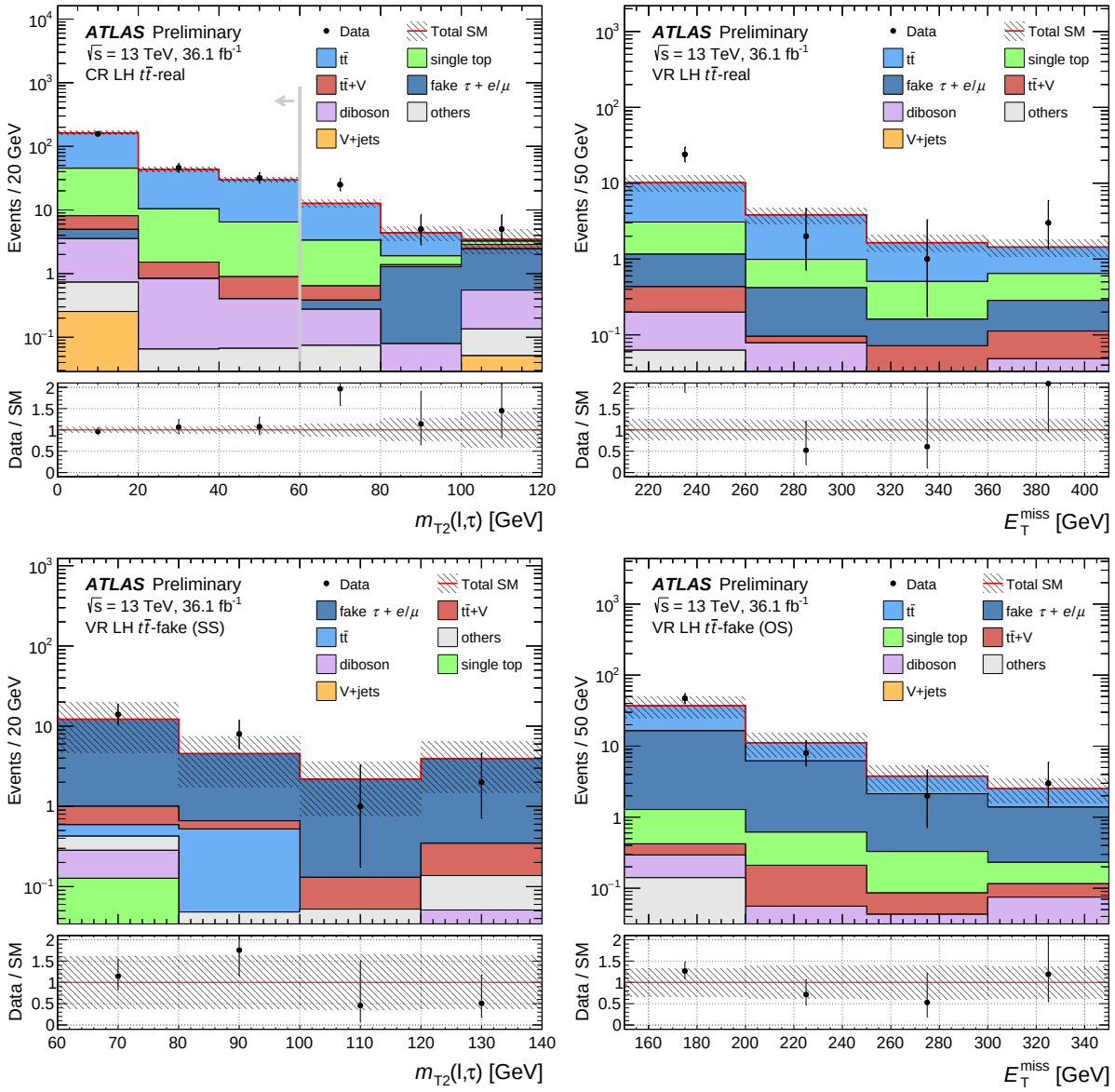

FIG. 2. Distributions of $m_{\mathrm{T2}}(\ell,\tau)$ (left) and $E_{\mathrm{T}}^{\mathrm{miss}}$ (right) in the control region and the validation regions of the lep-had channel, CR LH $t\bar{t}$-real (top left), VR LH $t\bar{t}$-real (top right), VR LH $t\bar{t}$-fake (SS) (bottom left), and VR LH $t\bar{t}$-fake (OS) (bottom right). The vertical line and arrow in the top-left plot indicate the $m_{\mathrm{T2}}(\ell,\tau)$ requirement of CR LH $t\bar{t}$-real, which is not applied in this plot. The stacked histograms show the various SM background contributions. The hatched band indicates the total statistical and systematic uncertainty on the SM background. The total background from events with a fake tau lepton in the lep-had channel (fake $\tau + e/\mu$) is obtained from the fake-factor method. The right-most bin includes the overflow.

The measurement region in which the fake factors are determined is based on the lep-had preselection. Events are selected where the tau lepton has the same charge as the light lepton to increase the fraction of fake tau leptons. The largest contribution to the events with fake tau leptons in the signal region, which will be estimated with the fake-factor method, is from $t\bar{t}$ production. Therefore, a requirement of $E_{\mathrm{T}}^{\mathrm{miss}} > 100\,\mathrm{GeV}$ is applied and at least one b-tagged jet required to obtain a high purity in $t\bar{t}$ events also in the measurement region. Finally, $m_{\mathrm{T2}}(\ell,\tau) < 60\,\mathrm{GeV}$ is required to make the measurement region orthogonal to the same-sign validation region VR LH $t\bar{t}$-fake (SS), in which good performance of the estimate is found. The fake factors measured in this region vary between 0.22 (0.042) and 0.085 (0.009) for 1-prong (3-prong) tau leptons as a function of p_{T}.

6.2 Had-Had Channel

TABLE IV. Definitions of the $t\bar{t}$ control and validation regions and the signal region in the had-had channel. A dash means that no requirement on this variable is applied. The brackets indicate a range that the variable is required to lie in. A common preselection as given in Table II for the had-had channel is applied.

	CR HH $t\bar{t}$-fake	CR HH $t\bar{t}$-real	VR HH $t\bar{t}$-fake	VR HH $t\bar{t}$-real	SR HH
charge(τ_1,τ_2)	—	opposite	—	opposite	opposite
$m_{\mathrm{T2}}(\tau_1,\tau_2)$	$< 30\,\mathrm{GeV}$	$< 30\,\mathrm{GeV}$	[30, 80] GeV	[30, 80] GeV	$> 80\,\mathrm{GeV}$
$E_{\mathrm{T}}^{\mathrm{miss}}$	$> 120\,\mathrm{GeV}$	$> 120\,\mathrm{GeV}$	$> 160\,\mathrm{GeV}$	$> 160\,\mathrm{GeV}$	$> 200\,\mathrm{GeV}$
$m_{\mathrm{T}}(\tau_1)$	$< 70\,\mathrm{GeV}$	$> 70\,\mathrm{GeV}$	$< 100\,\mathrm{GeV}$	$> 100\,\mathrm{GeV}$	—
$m(\tau_1,\tau_2)$	$> 70\,\mathrm{GeV}$	$> 70\,\mathrm{GeV}$	—	—	—

Two control and two validation regions are defined for the background with pair production of a top and an anti-top quark in the had-had channel. In all of these regions, the preselection requirements for the had-had channel from Table II are applied.

As in the lep-had channel, the sequence of control regions, validation regions, and signal region is ordered by increasing m_{T2}, the main discriminating variable. The CRs are restricted to $m_{\mathrm{T2}} < 30\,\mathrm{GeV}$, and the SR starts at $m_{\mathrm{T2}} > 80\,\mathrm{GeV}$. The VRs cover the intermediate phase-space region $30\,\mathrm{GeV} < m_{\mathrm{T2}} < 80\,\mathrm{GeV}$, so that the extrapolation in m_{T2} from the CRs to the SR can be validated here. A separation between events with real and fake tau leptons can be achieved using the transverse mass calculated from the leading tau and the missing transverse momentum. Events with fake tau leptons dominate at low values of m_{T}; events with real tau leptons tend to have higher values of m_{T}. In the signal region, the two tau leptons are required to have opposite charge, but since in events with a fake tau lepton the relative sign of the electric charges of the tau leptons is random, the number of events with fake tau leptons in the fake CR and VRs can be increased by not imposing this requirement. Also, the bound on $E_{\mathrm{T}}^{\mathrm{miss}}$ is lowered to 120 GeV to increase the number of events in the CRs. A requirement on the invariant mass of the tau-lepton pair suppresses Z + jets events and increases the purity in $t\bar{t}$ events in the CRs. Table IV summarizes the definitions of the CRs and VRs in the had-had channel.

In Fig. 3, four distributions of the main discriminating variables $m_{\mathrm{T2}}(\ell,\tau)$ and $E_{\mathrm{T}}^{\mathrm{miss}}$ are shown, here in the two CRs and two VRs of the had-had channel. The estimates for $t\bar{t}$ production, separated by whether the tau leptons are real or fake, and for $t\bar{t}+V$ and diboson production are scaled with the normalization factors obtained from the background fit (cf. Table VIII). The background process "$t\bar{t}$ (fake τ)" includes both events with one real and one fake tau lepton and two fake tau leptons.

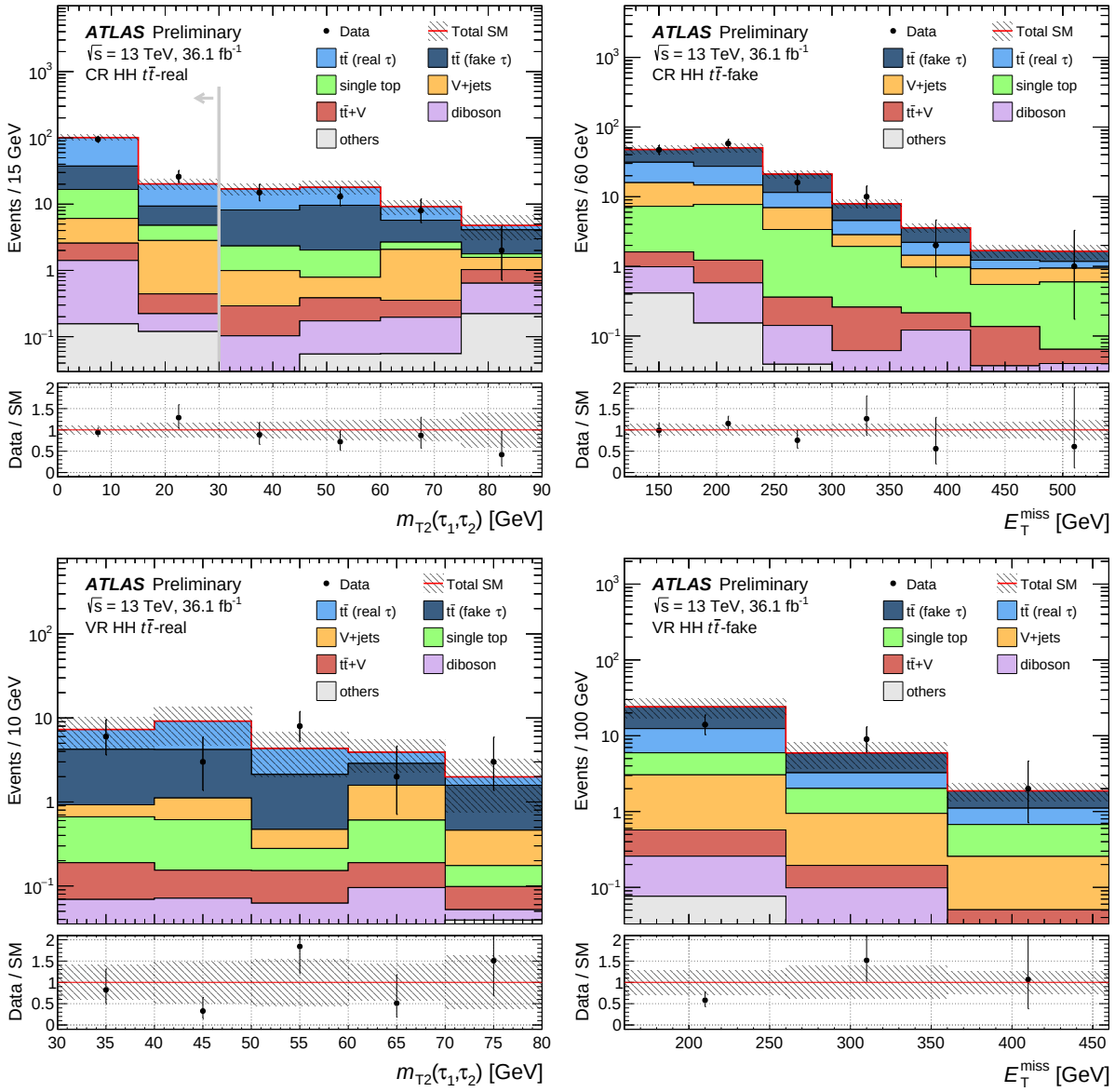

FIG. 3. Distributions of $m_{\mathrm{T2}}(\tau_1,\tau_2)$ (left) and $E_{\mathrm{T}}^{\mathrm{miss}}$ (right) in two control and two validation regions in the had-had channel, CR HH $t\bar{t}$-real (top left), CR HH $t\bar{t}$-fake (top right), VR HH $t\bar{t}$-real (bottom left), and VR HH $t\bar{t}$-fake (bottom right). The vertical line and arrow in the top-left plot indicate the $m_{\mathrm{T2}}(\tau_1,\tau_2)$ requirement of CR HH $t\bar{t}$-real, which is not applied in this plot. The stacked histograms show the various SM background contributions. The hatched band indicates the total statistical and systematic uncertainty on the SM background. The right-most bin includes the overflow. In the lower left plot, the overflow contribution is zero because VR HH $t\bar{t}$-real has an upper requirement on m_{T2}.

The relative contribution of events which are selected by either of the two triggers used in the had-had channel (cf. Sec. 5.1) varies between the control and validation regions and the signal region, as the fraction of events selected by the $E_{\mathrm{T}}^{\mathrm{miss}}$ trigger becomes higher with increasing $E_{\mathrm{T}}^{\mathrm{miss}}$ requirement. The normalization factors were therefore recomputed for the two sets of events selected exclusively by one of the two triggers. They were found to be compatible within their statistical uncertainties, showing that there is no dependence of the normalization factors on the trigger selection. This is also confirmed by the good agreement of data and predicted background yields in the validation regions when the normalization factors derived in the contol regions are applied.

6.3 Common Control Regions

TABLE V. Definition of the $t\bar{t}+V$ and VV control regions. The total number of signal leptons (e, μ or τ_h) is given by n_{lepton}, and n_{SFOS} is the number of lepton pairs with the same flavor and opposite charge. A dash means that no requirement on this variable is applied. The brackets indicate a range that the variable is required to lie in.

	CR $t\bar{t}+V$	CR VV
$p_{\mathrm{T}}(\mathrm{jet}_2)$	$> 26\,\mathrm{GeV}$	$> 26\,\mathrm{GeV}$
n_{SFOS}	≥ 1	≥ 1
m_Z^{closest}	$[80, 100]\,\mathrm{GeV}$	$[80, 100]\,\mathrm{GeV}$
$n_{b\text{-jets}}$	≥ 2	0
n_{lepton}	≥ 3	≥ 2
$n_{\mathrm{lepton}} + n_{\mathrm{jet}}$	≥ 6	—
$E_{\mathrm{T}}^{\mathrm{miss}} / \sqrt{H_{\mathrm{T}}}$	—	$> 15\ \sqrt{\mathrm{GeV}}$
$m_{\mathrm{T2}}(\ell,\ell)$	—	$> 120\,\mathrm{GeV}$

The definitions of the CR for events with $t\bar{t}$ production in association with a vector boson, CR $t\bar{t}+V$, and of the CR for events with diboson processes, CR VV, are given in Table V. They do not use the common preselection described in Sec. 5.1 but select events with at least two signal leptons (e, μ or τ_h). These events also need to have fired the single-lepton trigger and the respective trigger plateau requirement is applied as described in Sec. 5.1, so that at least one light lepton must be among the two leptons. Two jets must be present with $p_{\mathrm{T}} > 26\,\mathrm{GeV}$. No b-tagged jets are allowed in CR VV, whereas in CR $t\bar{t}+V$ at least two b-tagged jets are required to select events with top-quark decays.

The $t\bar{t}+V$ background in the signal region mostly consists of events in which a $t\bar{t}$ pair is produced in association with a Z boson that decays into two neutrinos providing large $E_{\mathrm{T}}^{\mathrm{miss}}$. This type of background cannot easily be separated from other backgrounds, in particular pure $t\bar{t}$ production, so that instead a CR enriched in $t\bar{t}+Z$ with $Z \to \ell\ell$ is used. It is then assumed that the normalization factor derived for this process is also valid for the Z decaying into neutrinos. Furthermore, as events with four or more leptons are too rare to make a CR, the CR $t\bar{t}+V$ requires only one additional, third signal lepton.

To select events with Z-boson decays, the invariant mass of all same flavor, opposite sign (SFOS) lepton pairs in the event is calculated. The pair with invariant mass closest to the mass of the Z boson, m_Z^{closest}, is selected and assumed to originate from the Z-boson decay. Only events where m_Z^{closest} is within about 10 GeV of the Z-boson mass are selected. As the invariant mass computed from the visible decay products of a Z boson into hadronically decaying tau leptons is smaller than the Z-boson mass, this in effect removes most of the events with tau lepton pairs. After applying these requirements, there is still a

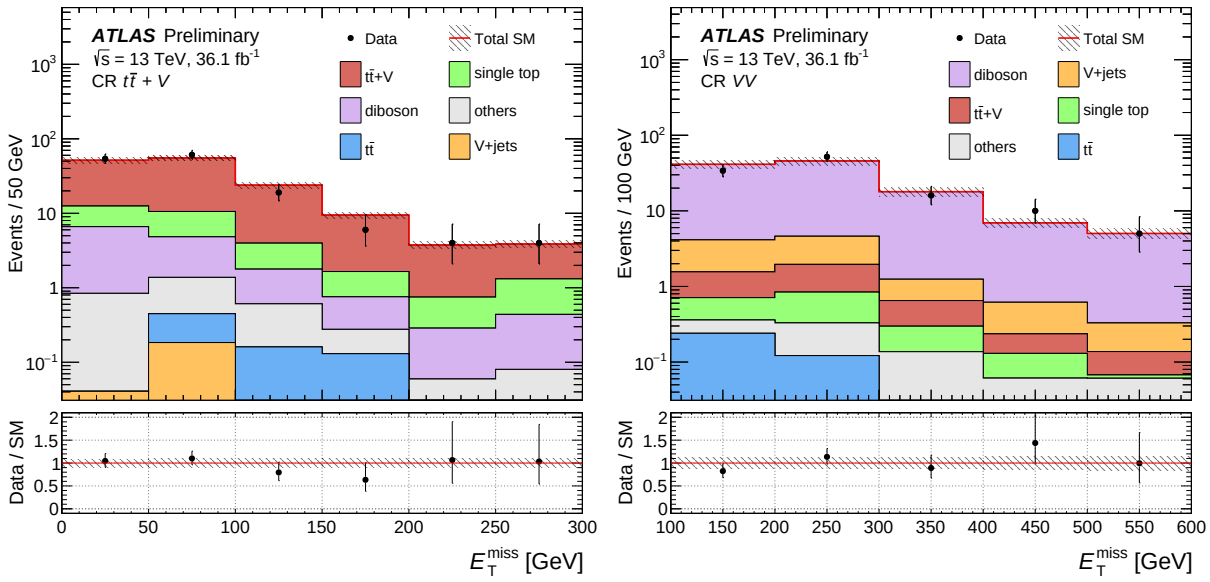

FIG. 4. Distributions of $E_{\mathrm{T}}^{\mathrm{miss}}$ in CR $t\bar{t}+V$ (left) and CR VV (right). The hatched band indicates the total statistical and systematic uncertainty on the SM background. The right-most bin includes the overflow.

sizable contribution from $Z+$jets events, where the SFOS pair originates from the Z boson and one of the jets is faking a tau lepton. Requiring the total number of leptons and jets to be at least six gives a small increase in the purity in $t\bar{t}+Z$ events in this region.

Events with diboson production entering the signal regions mostly have either two or three charged leptons. Events with four leptons are negligible in both channels. A CR for diboson production based on a tau-lepton selection would suffer from a high contamination from events in which a W boson is produced in association with jets, one of which fakes a hadronically decaying tau lepton. Therefore, the CR selection is based on light leptons and makes use of m_{T2} and the significance of the $E_{\mathrm{T}}^{\mathrm{miss}}$, measured as $E_{\mathrm{T}}^{\mathrm{miss}}/\sqrt{H_{\mathrm{T}}}$, to suppress $Z+$jets events. The requirement on m_Z^{closest} is used to suppress signal contamination, which otherwise becomes non-negligible for small mass differences between the top squark and tau slepton in the simplified model. Figure 4 shows the distribution of $E_{\mathrm{T}}^{\mathrm{miss}}$ in CR $t\bar{t}+V$ and in CR VV with the normalization factors from the background fit (cf. Table VIII) applied. The lower bins of $E_{\mathrm{T}}^{\mathrm{miss}}$ in CR VV which are not shown in the right plot are empty due to the requirement on $E_{\mathrm{T}}^{\mathrm{miss}}/\sqrt{H_{\mathrm{T}}}$.

7 Systematic Uncertainties

Experimental systematic uncertainties are taken into account for all simulated background and signal samples. For leptons, experimental systematic uncertainties arise from the reconstruction and identification efficiencies, and for electrons and muons also from the isolation efficiency. For jets, additional uncertainties from the pile-up subtraction, pseudorapidity intercalibration, flavor composition, and punch-through effects, as well as uncertainties in the flavor-tagging and jet-vertex tagging efficiencies are considered using a reduced set of nuisance parameters [87]. Uncertainties in the energy resolution and calibration are taken into account for all physics objects. $E_{\mathrm{T}}^{\mathrm{miss}}$ has an additional uncertainty due to the contribution

of the soft-track term. The fast detector simulation used for the signal samples brings additional uncertainties for jets and tau leptons. Further sources of experimental systematic uncertainties are the pile-up reweighting of simulated events to cover the uncertainty on the ratio between the predicted and measured inelastic cross-section, and the measurement of the trigger scale factors.

Several sources of uncertainty are found to be important for the background estimate obtained from the fake-factor method: statistical uncertainties in the fake factors from the number of events in the measurement region and the number of AntiID events in the respective target selection are propagated into the uncertainty on the final estimate. Further uncertainties in the fake factors arise from the contribution of multi-jet events, which enter the measurement region due to the softer requirement on $E_{\mathrm{T}}^{\mathrm{miss}}$ with respect to the other lep-had selections, and the subtraction of events with real tau leptons. The former uncertainty is estimated by varying the $E_{\mathrm{T}}^{\mathrm{miss}}$ requirement of the measurement region, the latter by scaling the simulation-based estimate for these events by up to $\pm 40\,\%$. An uncertainty from the choice of the AntiID working point is derived by reevaluating and comparing the estimate obtained from the fake-factor method for different values of the AntiID working point. Finally, the impact of the extrapolation of the fake factor in m_{T2} is translated into an uncertainty by comparing fake factors obtained for different ranges of m_{T2} in the measurement region. This is the dominant source of uncertainty for the fake-factor method.

Uncertainties in the theoretical modelling are evaluated for the dominant processes of the analysis selections. For the hard-scatter modelling of the $t\bar{t}$ and single-top processes, systematic uncertainties are estimated by comparing the hard-process generation between Powheg and aMC@NLO, both interfaced with Herwig++ for the showering, while uncertainties in the fragmentation and hadronization are estimated from a comparison of samples where the hard scattering is done with Powheg, interfaced with Herwig++ or Pythia, respectively. Uncertainties in additional radiation are obtained through a variation of the generator settings, such as the produced shower radiation, the factorization and renormalization scales and the NLO radiation. An uncertainty in the treatment of the interference subtraction of single-top quark production in the Wt channel and $t\bar{t}$ production at next-to-leading order is estimated as the difference of diagram-removal and diagram-subtraction schemes [88, 89].

For $t\bar{t}+V$ production, the uncertainty in the hard-scatter modelling is assessed by comparing the nominal aMC@NLO interfaced with Pythia to Sherpa; for VV production, the nominal Sherpa is compared to Powheg interfaced with Pythia for the showering. For both $t\bar{t}+V$ and VV, additional variations of the internal parameters of the generators for the factorization and hadronization scales are evaluated.

A cross section uncertainty of $5\,\%$ is considered for $Z+$jets, $W+$jets, and single-top quark production because their yields are not normalized in control regions. The uncertainty on the integrated luminosity described in Sec. 3 is also applied to all backgrounds that are taken directly from simulation. In all regions, the statistical uncertainties of the MC simulations and the uncertainties on the normalization factors are taken into account.

The full set of systematic uncertainties in the total background yields is summarized in Table VI. The largest sources of experimental systematic uncertainties in both channels include the jet and tau energy calibration, the pile-up reweighting and the $E_{\mathrm{T}}^{\mathrm{miss}}$ measurement. In the lep-had channel, the dominant contribution to the overall systematic uncertainty comes from the uncertainties in the fake-factor method. The advantage of using a data-driven method for the largest part of the background is the moderate total uncertainty in this channel compared to the had-had channel, where simulation is used to extrapolate from the control region. In the had-had channel, the uncertainty in the total background estimate is driven by the uncertainty in the estimate of $t\bar{t}$ events with fake tau leptons, the largest background contribution. The

TABLE VI. Relative systematic uncertainties on the estimated number of background events in the signal regions (left: lep-had, right: had-had channel). In the lower part of the table, a breakdown into different categories is given: all jet- and tau-related systematics are added into a respective combined value, while the smaller experimental uncertainties from electrons, muons, flavor-tagging, $E_{\mathrm{T}}^{\mathrm{miss}}$, and pile-up reweighting are combined into "Other experimental". The percentage values give the relative post-fit uncertainties on the total expected background yield. The individual contributions do not add up to the total given in the first row due to the correlations between the individual systematic uncertainties.

	SR LH	SR HH
Total systematic uncertainty	± 29 %	± 53 %
Fake-factor method	± 23 %	—
Jet-related	± 9.3 %	± 36 %
Tau-related	± 7.2 %	± 32 %
Other experimental	± 6.1 %	± 12 %
Theory modelling	± 8.3 %	± 20 %
MC statistics	± 7.5 %	± 17 %
Normalization factors	± 4.8 %	± 14 %
Luminosity	± 0.3 %	± 0.8 %

dominant effect is the systematic uncertainty in the tau energy scale and from jet mismodelling due to the MC-based residual pile-up correction, which significantly affect the extrapolation from the control to the signal region.

For the signal, in addition to the experimental uncertainties, theoretical uncertainties in the cross sections are taken from an envelope of cross section predictions using different PDF sets and factorization and renormalization scales, as described in Ref. [90]. They vary between 13 % and 20 %, which is similar to the size of the experimental uncertainties on the signal.

8 Results

The statistical interpretation of the results is performed using the HistFitter framework [91] that carries out the fitting procedure based on a maximum-likelihood approach and the hypothesis tests utilizing the profile-likelihood ratio as a test statistic with asymptotic formulae [92]. All regions are treated as single bins in the likelihood fits, i.e. no shape information is used. Systematic uncertainties are implemented as nuisance parameters, taking into account potential correlations. The background fit uses the three CRs of the lep-had and the had-had channel and the two common CRs simultaneously. The normalization factors from the background fit are extrapolated to the VRs and SRs in order to obtain the background estimates in these regions, again accounting for correlations between systematic uncertainties.

The results from the background fit for the individual expected contributions of the SM processes and for their sum in the two signal regions are shown in Table VII, together with the observed yields from the analysis dataset with an integrated luminosity of 36.1 fb^{-1}. Table VIII summarizes the four normalization factors obtained from the background fit. Overall, they are compatible with unity. The observed data yields in the signal regions in Table VII are in agreement with the expected total background yields from SM processes in both the lep-had and the had-had channels. No significant excess is observed.

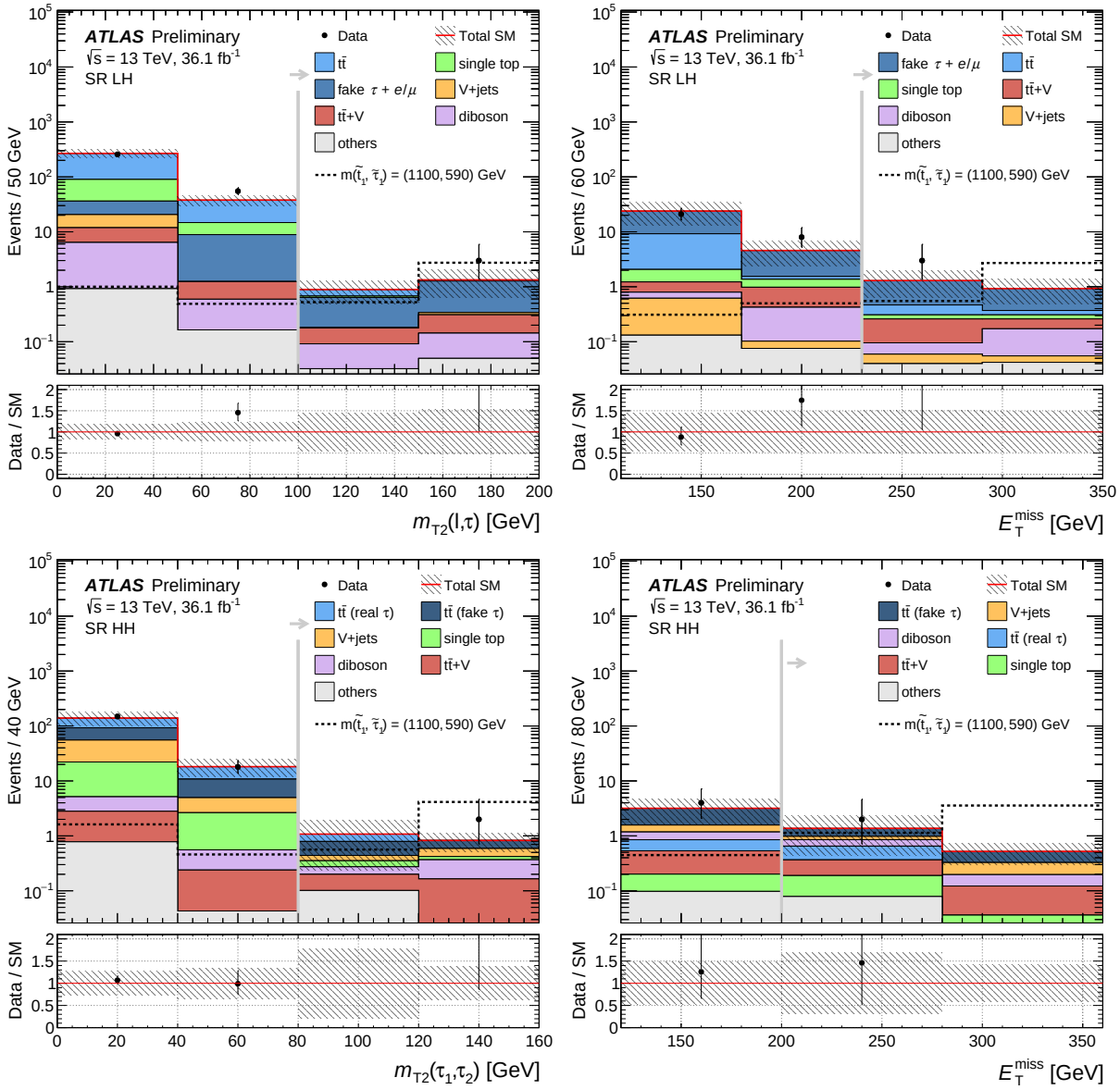

FIG. 5. Distributions of m_{T2} (left) and $E_{\mathrm{T}}^{\mathrm{miss}}$ (right) in the signal regions of the lep-had channel (top) and had-had channel (bottom) before the respective selection requirements, indicated by the vertical line and arrow, are applied. The stacked histograms show the various SM background contributions. The total background from events with a fake tau lepton in the lep-had channel (fake $\tau + e/\mu$) is obtained from the fake-factor method. The hatched band indicates the total statistical and systematic uncertainty on the SM background. The error bars on the black data points represent the statistical uncertainty on the data yields. The dashed line shows the expected additional yields from a benchmark signal model. The right-most bin includes the overflow.

TABLE VII. Expected numbers of events for the SM background processes from the background fit and observed event yield in data for the signal regions in the lep-had and had-had channel, given for an integrated luminosity of 36.1 fb^{-1}. The expected yield for the signal model with $m_{\tilde{t}_1} = 1100\,\text{GeV}$ and $m_{\tilde{\tau}_1} = 590\,\text{GeV}$ is shown for comparison. The uncertainties include both statistical and systematic uncertainties and are truncated at zero. The total background from events with a fake tau lepton in the lep-had channel (fake $\tau + e/\mu$) is obtained from the fake-factor method.

	SR LH	SR HH
Observed events	3	2
Total background	2.2 ± 0.6	1.9 ± 1.0
fake $\tau + e/\mu$	1.4 ± 0.5	—
$t\bar{t}$ (fake τ)	—	$0.6 \pm {}^{0.7}_{0.6}$
$t\bar{t}$ (real τ)	0.22 ± 0.12	$0.28 \pm {}^{0.30}_{0.28}$
$t\bar{t} + V$	0.25 ± 0.14	0.26 ± 0.12
diboson	0.15 ± 0.11	0.28 ± 0.13
single-top	$0.10 \pm {}^{0.24}_{0.10}$	0.13 ± 0.11
V + jets	0.033 ± 0.011	0.26 ± 0.06
others	0.082 ± 0.020	0.09 ± 0.04
signal	3.3 ± 0.7	4.7 ± 1.2
($m(\tilde{t}_1) = 1100\,\text{GeV}$, $m(\tilde{\tau}_1) = 590\,\text{GeV}$)		

TABLE VIII. Normalization factors obtained from the background-only fit. The normalization factor on $t\bar{t}$ events with fake tau leptons is only relevant for the had-had channel.

Process	Normalization factor
diboson	$1.0 \pm {}^{0.6}_{0.3}$
$t\bar{t} + V$	$1.39 \pm {}^{0.23}_{0.23}$
$t\bar{t}$ (fake τ)	$1.2 \pm {}^{0.4}_{0.4}$
$t\bar{t}$ (real τ)	$0.81 \pm {}^{0.20}_{0.19}$

Figure 5 shows the distributions of m_{T2} and $E_{\text{T}}^{\text{miss}}$ in the signal regions of the lep-had channel and had-had channel. All selection requirements are applied, except that on the variable shown in the plot, which is instead indicated by the vertical line and arrow.

The complete analysis results are displayed in Fig. 6, which shows the data yields (N_{obs}) and background expectations (N_{exp}) in all analysis regions, and the resulting pulls $(N_{\text{obs}} - N_{\text{exp}})/\sigma_{\text{exp}}$ in the validation and signal regions, where σ_{exp} includes the total uncertainty on the background estimate and the Poisson uncertainty on the data yield. The pulls in all but one validation region are below one standard deviation. In the VR targeting $t\bar{t}$ events with a real tau lepton in the lep-had channel, an upwards fluctuation of around 2.3 standard deviations is observed. However, the distribution of m_{T2} in this VR (top left plot in Fig. 2) shows that the excess is confined to the single bin farthest away from the signal region ($60\,\text{GeV} < m_{\text{T2}}(\ell,\tau) < 80\,\text{GeV}$), and therefore inconsistent with a signal.

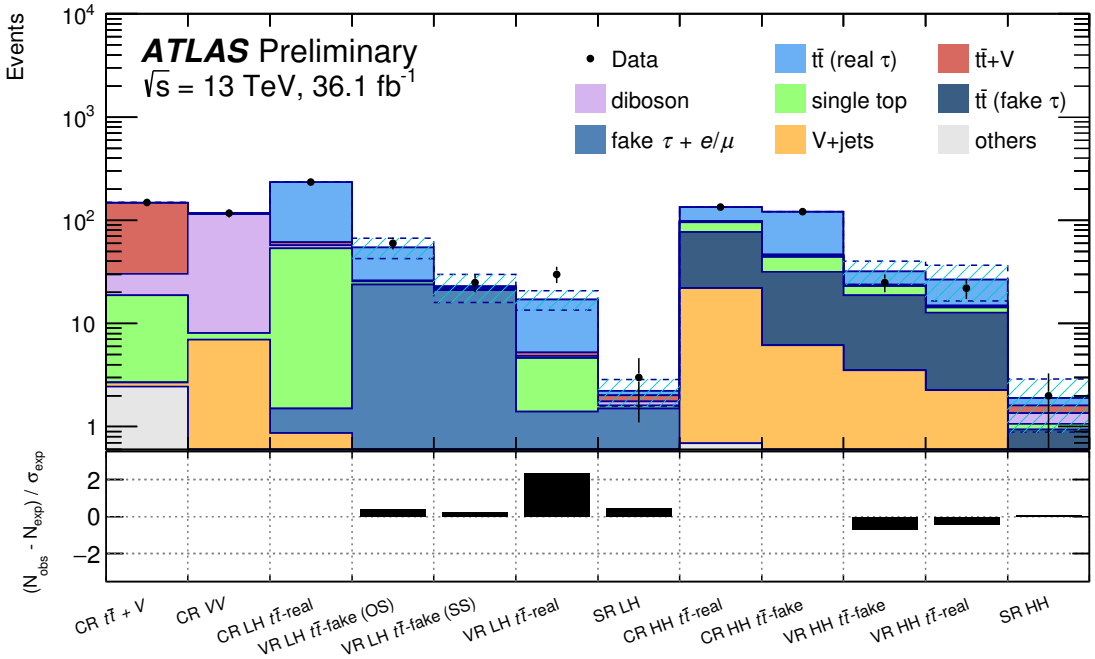

FIG. 6. Data yields and background expectation in all analysis regions from the lep-had and had-had channel (top) and the resulting pulls in the validation and signal regions (bottom). The hatched band gives the total statistical and systematic uncertainty on the background estimate in each bin. The pulls in the control regions are small by construction as the normalization factors obtained from the fit are applied. The contribution of $t\bar{t}$ events to CR $t\bar{t}+V$ and CR VV is below a percent and not drawn here.

8.1 Interpretation

In the absence of a significant excess beyond the SM predictions in either signal region, the result is interpreted in terms of an exclusion limit on the masses of the particles in the simplified signal model. In contrast to the background fit, the combined likelihood fit that is done to derive the model-dependent exclusion limits allows for signal contamination in the CRs and includes the signal region. The CL_s values [93], representing the compatibility of the signal hypothesis with the observation, are derived from hypotheses tests using the post-fit statistical model.

Figure 7 shows the expected and observed exclusion-limit contours at 95 % confidence level (CL) obtained from the statistical combination of the lep-had and had-had channels with full experimental and theory systematic uncertainties. Top-squark masses up to 1.16 TeV and tau-slepton masses up to 1.00 TeV are excluded, which improves the previous result of the ATLAS analysis of 20 fb^{-1} of LHC data at $\sqrt{s}$ = 8 TeV [22] by almost a factor two in both mass parameters. The had-had channel has better sensitivity than the lep-had channel over the whole grid, but the combination helps to improve the sensitivity, in particular for large tau-slepton masses. For low tau-slepton masses, the sensitivity decreases and the limit on the top-squark mass is lower than at higher tau-slepton masses because the tau leptons from the tau-slepton decay become less energetic, which reduces the acceptance of the analysis selection.

In addition to the model-dependent limits above, the analysis results are also interpreted in terms of model-independent upper limits on the number of events from non-Standard-Model processes in the signal region, S^{95}_{obs}. Dividing this number by the integrated luminosity of the dataset gives an upper limit on

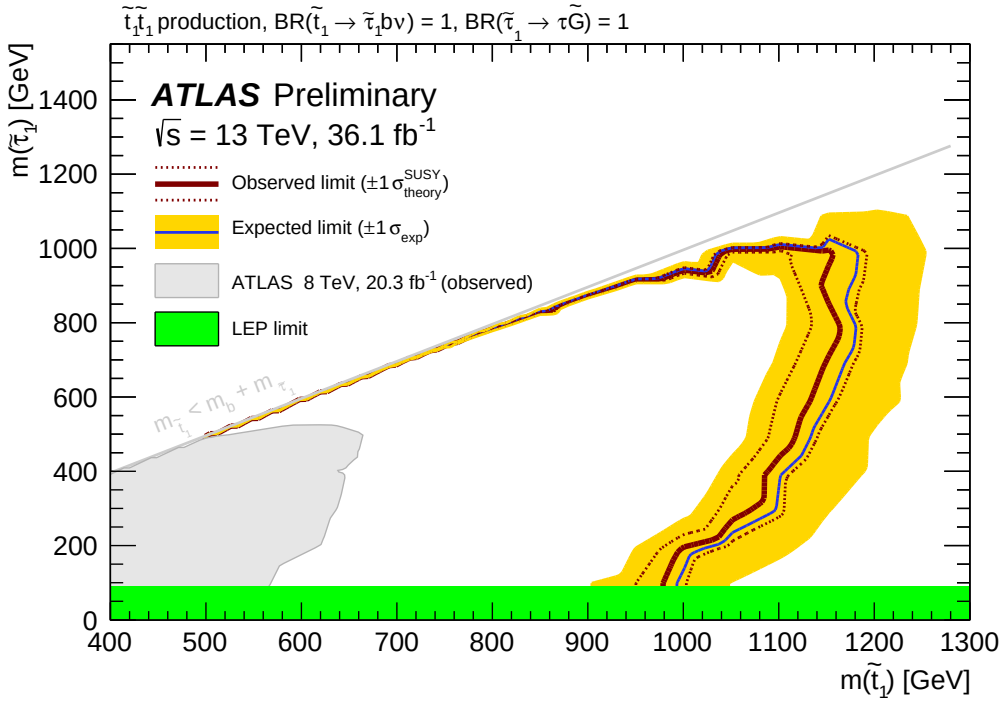

FIG. 7. Expected (solid blue line) and observed (solid red line) exclusion-limit contours at 95 % confidence level, for the statistical combination of the lep-had and had-had channels, using full experimental and theory systematic uncertainties. The yellow band shows one-sigma variations around the expected limit contour, including all uncertainties except the theoretical uncertainty on the signal cross section. The dotted red lines indicate how the observed limit moves when varying the signal cross section up or down by the corresponding uncertainty in the theoretical value. For comparison, the plot also shows the observed exclusion contour from the ATLAS Run-1 analysis [22] as area shaded in gray and the limit on the mass of the tau slepton (for a massless LSP) from the LEP experiments [23] as green band.

TABLE IX. Left to right: observed 95 % CL upper limits on the visible cross section ($\langle\epsilon\sigma\rangle^{95}_{\text{obs}}$) and on the number of signal events (S^{95}_{obs}). The third column (S^{95}_{exp}) shows the expected 95 % CL upper limit on the number of signal events, given the expected number (and $\pm 1\sigma$ excursions on the expectation) of background events. The last two columns indicate the CL_b value, i.e. the confidence level observed for the background-only hypothesis, and the discovery p-value ($p(s = 0)$) and the corresponding significance (Z).

Signal channel	$\langle\epsilon\sigma\rangle^{95}_{\text{obs}}$[fb]	S^{95}_{obs}	S^{95}_{exp}	CL_b	$p(s = 0)$ (Z)
SR LH	0.15	5.4	$4.5^{+2.6}_{-1.5}$	0.65	0.32 (0.47)
SR HH	0.13	4.7	$4.6^{+2.5}_{-1.5}$	0.52	0.48 (0.05)

the visible signal cross section, $\langle \epsilon\sigma \rangle^{95}_{\text{obs}}$, defined as the product of acceptance, reconstruction efficiency and signal cross section. The derivation of these limits uses the background estimates in the SRs from the background-only fit, thus assuming no contamination by a potential signal in the CRs. The model-independent limits are shown in Table IX separately for the two channels, again computed using the CL_s prescription. The lep-had channel yields a slightly lower expected limit than the had-had channel despite the larger expected SM background because the total uncertainty is smaller. On the other hand, the mild excess of observed events is larger in the lep-had channel, so that the observed model-independent limit is lower for the had-had channel than for the lep-had channel, and the p-value for the background-only hypothesis in the lep-had channel is smaller.

9 Conclusion

In this note, a search for the direct pair production of supersymmetric top squarks in final states with two tau leptons, jets identified as originating from b-hadron decays, and missing transverse momentum is presented.

The search uses a dataset with proton–proton collisions at a center-of-mass energy of $\sqrt{s} = 13\,\text{TeV}$, which was recorded with the ATLAS detector at the Large Hadron Collider in 2015 and 2016 and has a total integrated luminosity of $36.1\,\text{fb}^{-1}$. Two exclusive channels are considered, which select events with either two hadronically decaying tau leptons or one hadronically decaying tau lepton and one electron or muon. Good agreement between the Standard Model predictions and the event yields observed in data is found in the signal region of each channel. The analysis results are therefore interpreted in terms of upper limits on the production of supersymmetric particles. In a simplified model with production of two top squarks, each decaying via a tau slepton to a nearly massless gravitino as the lightest supersymmetric particle, masses up to $m(\tilde{t}_1) = 1.16\,\text{TeV}$ and $m(\tilde{\tau}_1) = 1.00\,\text{TeV}$ are excluded at 95 % confidence level, extending previous limits in this model by almost a factor two. Model-independent limits allow the exclusion of visible cross sections of 0.15 (0.13) fb in the lep-had (had-had) channel for production of events beyond the Standard Model in the studied final state.

References

[1] Yu. A. Golfand and E. P. Likhtman,
Extension of the Algebra of Poincare Group Generators and Violation of p Invariance,
JETP Lett. **13** (1971) 323,
URL: http://www.jetpletters.ac.ru/ps/1584/article_24309.pdf.

[2] D. V. Volkov and V. P. Akulov, *Is the Neutrino a Goldstone Particle?* Phys. Lett. B **46** (1973) 109.

[3] J. Wess and B. Zumino, *Supergauge Transformations in Four-Dimensions*,
Nucl. Phys. B **70** (1974) 39.

[4] J. Wess and B. Zumino, *Supergauge Invariant Extension of Quantum Electrodynamics*,
Nucl. Phys. B **78** (1974) 1.

[5] S. Ferrara and B. Zumino, *Supergauge Invariant Yang-Mills Theories*,
Nucl. Phys. B **79** (1974) 413.

[6] A. Salam and J. A. Strathdee, *Supersymmetry and Nonabelian Gauges*,
Phys. Lett. B **51** (1974) 353.

[7] S. P. Martin, *A Supersymmetry primer*, (1997), [Adv. Ser. Direct. High Energy Phys.18,1(1998)],
arXiv: hep-ph/9709356 [hep-ph].

[8] G. R. Farrar and P. Fayet, *Phenomenology of the Production, Decay, and Detection of New Hadronic States Associated with Supersymmetry*, Phys. Lett. B **76** (1978) 575.

[9] M. Dine and W. Fischler,
A Phenomenological Model of Particle Physics Based on Supersymmetry,
Phys. Lett. B **110** (1982) 227.

[10] L. Alvarez-Gaume, M. Claudson, and M. B. Wise, *Low-Energy Supersymmetry*,
Nucl. Phys. B **207** (1982) 96.

[11] C. R. Nappi and B. A. Ovrut, *Supersymmetric Extension of the SU(3) x SU(2) x U(1) Model*,
Phys. Lett. B **113** (1982) 175.

[12] M. Asano, H. D. Kim, R. Kitano, and Y. Shimizu, *Natural supersymmetry at the LHC*,
JHEP **12** (2010) 019, arXiv: 1010.0692.

[13] J. Alwall, P. Schuster, and N. Toro,
Simplified models for a first characterization of new physics at the LHC,
Phys. Rev. D **79** (2009) 075020, arXiv: 0810.3921 [hep-ph].

[14] D. Alves, *Simplified models for LHC new physics searches*,
J. Phys. G **39** (2012) 105005, ed. by N. Arkani-Hamed et al., arXiv: 1105.2838 [hep-ph].

[15] K. Inoue, A. Kakuto, H. Komatsu, and S. Takeshita,
Aspects of Grand Unified Models with Softly Broken Supersymmetry,
Prog. Theor. Phys. **68** (1982) 927, [Erratum: Prog. Theor. Phys.70,330(1983)].

[16] J. R. Ellis and S. Rudaz, *Search for Supersymmetry in Toponium Decays*,
Phys. Lett. B **128** (1983) 248.

[17] ATLAS Collaboration, *ATLAS Run 1 searches for direct pair production of third-generation squarks at the Large Hadron Collider*, Eur. Phys. J. C **75** (2015) 510,
arXiv: 1506.08616 [hep-ex].

[18] ATLAS Collaboration, *Search for top squarks in final states with one isolated lepton, jets, and missing transverse momentum in* $\sqrt{s} = 13$ *TeV pp collisions with the ATLAS detector*, Phys. Rev. D **94** (2016) 052009, arXiv: 1606.03903 [hep-ex].

[19] ATLAS Collaboration, *Search for direct top squark pair production in final states with two leptons in* $\sqrt{s} = 13$ *TeV pp collisions with the ATLAS detector*, submitted to EPJC (2017), arXiv: 1708.03247 [hep-ex].

[20] CMS Collaboration, *Search for direct production of supersymmetric partners of the top quark in the all-jets final state in proton-proton collisions at* $\sqrt{s} = 13$ TeV, JHEP **10** (2017) 005, arXiv: 1707.03316 [hep-ex].

[21] CMS Collaboration, *Search for top squark pair production in pp collisions at* $\sqrt{s} = 13$ TeV *using single lepton events*, JHEP **10** (2017) 019, arXiv: 1706.04402 [hep-ex].

[22] ATLAS Collaboration, *Search for direct top squark pair production in final states with two tau leptons in pp collisions at* $\sqrt{s} = 8$ *TeV with the ATLAS detector*, Eur. Phys. J. C **76** (2016) 81, arXiv: 1509.04976 [hep-ex].

[23] The LEP2 SUSY Working Group and ALEPH, DELPHI, L3, OPAL Experiments, "Combined LEP Selectron/Smuon/Stau Results, 183-208 GeV," http://lepsusy.web.cern.ch/lepsusy/www/sleptons_summer04/slep_final.html, 2004.

[24] ATLAS Collaboration, *Search for the direct production of charginos, neutralinos and staus in final states with at least two hadronically decaying taus and missing transverse momentum in pp collisions at* $\sqrt{s} = 8$ *TeV with the ATLAS detector*, JHEP **10** (2014) 096, arXiv: 1407.0350 [hep-ex].

[25] ATLAS Collaboration, *Search for the electroweak production of supersymmetric particles in* $\sqrt{s} = 8$ *TeV pp collisions with the ATLAS detector*, Phys. Rev. D **93** (2016) 052002, arXiv: 1509.07152 [hep-ex].

[26] CMS Collaboration, *Search for pair production of tau sleptons in* $\sqrt{s} = 13$ TeV *pp collisions in the all-hadronic final state*, CMS-PAS-SUS-17-003, 2017, URL: https://cds.cern.ch/record/2273395.

[27] ATLAS Collaboration, *The ATLAS Experiment at the CERN Large Hadron Collider*, JINST **3** (2008) S08003.

[28] ATLAS Collaboration, *ATLAS Insertable B-Layer Technical Design Report*, CERN-LHCC-2010-013. ATLAS-TDR-19, 2010, URL: https://cds.cern.ch/record/1291633.

[29] ATLAS Collaboration, *Performance of the ATLAS trigger system in 2015*, Eur. Phys. J. C **77** (2017) 317, arXiv: 1611.09661 [hep-ex].

[30] E. Todesco and J. Wenninger, *Large Hadron Collider momentum calibration and accuracy*, Phys. Rev. Accel. Beams **20** (8 2017) 081003.

[31] ATLAS Collaboration, *Luminosity determination in pp collisions at* $\sqrt{s} = 8$ *TeV using the ATLAS detector at the LHC*, Eur. Phys. J. C **76** (2016) 653, arXiv: 1608.03953 [hep-ex].

[32] J. Alwall et al., *The automated computation of tree-level and next-to-leading order differential cross sections, and their matching to parton shower simulations*, JHEP **07** (2014) 079, arXiv: 1405.0301 [hep-ph].

[33] T. Sjöstrand, S. Mrenna, and P. Skands, *A brief introduction to PYTHIA 8.1*, Comput. Phys. Commun. **178** (2008) 852, arXiv: 0710.3820 [hep-ph].

[34] T. Sjöstrand et al., *An introduction to PYTHIA 8.2*, Comput. Phys. Commun. **191** (2015) 159, arXiv: 1410.3012 [hep-ph].

[35] ATLAS Collaboration, *ATLAS Pythia 8 tunes to 7 TeV data*, ATL-PHYS-PUB-2014-021, 2014, URL: https://cds.cern.ch/record/1966419.

[36] R. D. Ball et al., *Parton distributions with LHC data*, Nucl. Phys. B **867** (2013) 244, arXiv: 1207.1303 [hep-ph].

[37] L. Lönnblad and S. Prestel, *Merging multi-leg NLO matrix elements with parton showers*, JHEP **03** (2013) 166, arXiv: 1211.7278 [hep-ph].

[38] W. Beenakker, M. Krämer, T. Plehn, M. Spira, and P. M. Zerwas, *Stop production at hadron colliders*, Nucl. Phys. B **515** (1998) 3, arXiv: hep-ph/9710451.

[39] W. Beenakker et al., *Supersymmetric top and bottom squark production at hadron colliders*, JHEP **08** (2010) 098, arXiv: 1006.4771 [hep-ph].

[40] W. Beenakker et al., *Squark and gluino hadroproduction*, Int. J. Mod. Phys. A **26** (2011) 2637, arXiv: 1105.1110 [hep-ph].

[41] S. Alioli, P. Nason, C. Oleari, and E. Re, *A general framework for implementing NLO calculations in shower Monte Carlo programs: the POWHEG BOX*, JHEP **06** (2010) 043, arXiv: 1002.2581 [hep-ph].

[42] T. Sjöstrand, S. Mrenna, and P. Skands, *PYTHIA 6.4 physics and manual*, JHEP **05** (2006) 026, arXiv: hep-ph/0603175 [hep-ph].

[43] H.-L. Lai et al., *New parton distributions for collider physics*, Phys. Rev. D **82** (2010) 074024, arXiv: 1007.2241 [hep-ph].

[44] J. Pumplin et al., *New generation of parton distributions with uncertainties from global QCD analysis*, JHEP **07** (2002) 012, arXiv: hep-ph/0201195 [hep-ph].

[45] P. Z. Skands, *Tuning Monte Carlo generators: The Perugia tunes*, Phys. Rev. D **82** (2010) 074018, arXiv: 1005.3457 [hep-ph].

[46] M. Bähr et al., *Herwig++ physics and manual*, Eur. Phys. J. C **58** (2008) 639, arXiv: 0803.0883 [hep-ph].

[47] J. Bellm et al., *Herwig++ 2.7 Release Note*, (2013), arXiv: 1310.6877 [hep-ph].

[48] S. Gieseke, C. Röhr, and A. Siodmok, *Colour reconnections in Herwig++*, Eur. Phys. J. C **72** (2012) 2225, arXiv: 1206.0041 [hep-ph].

[49] R. D. Ball et al., *Parton distributions for the LHC Run II*, JHEP **04** (2015) 040, arXiv: 1410.8849 [hep-ph].

[50] D. J. Lange, *The EvtGen particle decay simulation package*, Nucl. Instrum. Meth. A **462** (2001) 152 .

[51] T. Gleisberg et al., *Event generation with SHERPA 1.1*, JHEP **02** (2009) 007, arXiv: 0811.4622 [hep-ph].

[52] S. Schumann and F. Krauss, *A Parton shower algorithm based on Catani-Seymour dipole factorisation*, JHEP **03** (2008) 038, arXiv: 0709.1027 [hep-ph].

[53] S. Agostinelli et al., *GEANT 4 — a simulation toolkit*, Nucl. Instrum. Meth. A **506** (2003) 250 .

[54] ATLAS Collaboration, *The ATLAS Simulation Infrastructure*, Eur. Phys. J. C **70** (2010) 823, arXiv: 1005.4568 [hep-ex].

[55] ATLAS Collaboration, *The simulation principle and performance of the ATLAS fast calorimeter simulation FastCaloSim*, ATL-PHYS-PUB-2010-013, 2010, URL: https://cds.cern.ch/record/1300517.

[56] ATLAS Collaboration, *Summary of ATLAS Pythia 8 tunes*, ATL-PHYS-PUB-2012-003, 2012, URL: https://cds.cern.ch/record/1474107.

[57] A. D. Martin, W. J. Stirling, R. S. Thorne, and G. Watt, *Parton distributions for the LHC*, Eur. Phys. J. C **63** (2009) 189, arXiv: 0901.0002 [hep-ph].

[58] ATLAS Collaboration, *Vertex Reconstruction Performance of the ATLAS Detector at* $\sqrt{s} = 13$ *TeV*, ATL-PHYS-PUB-2015-026, 2015, URL: https://cds.cern.ch/record/2037717.

[59] ATLAS Collaboration, *Properties of jets and inputs to jet reconstruction and calibration with the ATLAS detector using proton–proton collisions at* $\sqrt{s} = 13$ *TeV*, ATL-PHYS-PUB-2015-036, 2015, URL: https://cds.cern.ch/record/2044564.

[60] M. Cacciari, G. P. Salam, and G. Soyez, *The anti-k_t jet clustering algorithm*, JHEP **04** (2008) 063, arXiv: 0802.1189 [hep-ph].

[61] ATLAS Collaboration, *Jet energy scale measurements and their systematic uncertainties in proton-proton collisions at* $\sqrt{s} = 13$ *TeV with the ATLAS detector*, Phys. Rev. D **96** (2017) 072002, arXiv: 1703.09665 [hep-ex].

[62] ATLAS Collaboration, *Selection of jets produced in* 13 *TeV proton–proton collisions with the ATLAS detector*, ATLAS-CONF-2015-029, 2015, URL: https://cds.cern.ch/record/2037702.

[63] ATLAS Collaboration, *Performance of pile-up mitigation techniques for jets in pp collisions at* $\sqrt{s} = 8$ *TeV using the ATLAS detector*, Eur. Phys. J. C **76** (2016) 581, arXiv: 1510.03823 [hep-ex].

[64] ATLAS Collaboration, *Performance of b-jet identification in the ATLAS experiment*, JINST **11** (2016) P04008, arXiv: 1512.01094 [hep-ex].

[65] ATLAS Collaboration, *Optimisation of the ATLAS b-tagging performance for the 2016 LHC Run*, ATL-PHYS-PUB-2016-012, 2016, URL: https://cds.cern.ch/record/2160731.

[66] ATLAS Collaboration, *Reconstruction, Energy Calibration, and Identification of Hadronically Decaying Tau Leptons in the ATLAS Experiment for Run-2 of the LHC*, ATL-PHYS-PUB-2015-045, 2015, URL: https://cds.cern.ch/record/2064383.

[67] ATLAS Collaboration, *Identification and energy calibration of hadronically decaying tau leptons with the ATLAS experiment in pp collisions at* $\sqrt{s} = 8$ *TeV*, Eur. Phys. J. C **75** (2015) 303, arXiv: 1412.7086 [hep-ex].

[68] ATLAS Collaboration, *Measurement of the tau lepton reconstruction and identification performance in the ATLAS experiment using pp collisions at* $\sqrt{s} = 13$ *TeV*, ATLAS-CONF-2017-029, 2017, URL: https://cds.cern.ch/record/2261772.

[69] ATLAS Collaboration, *Electron efficiency measurements with the ATLAS detector using the 2015 LHC proton–proton collision data*, ATLAS-CONF-2016-024, 2016, URL: https://cds.cern.ch/record/2157687.

[70] ATLAS Collaboration, *Electron efficiency measurements with the ATLAS detector using 2012 LHC proton–proton collision data*, Eur. Phys. J. C **77** (2017) 195, arXiv: 1612.01456 [hep-ex].

[71] ATLAS Collaboration, *Muon reconstruction performance of the ATLAS detector in proton–proton collision data at* $\sqrt{s} = 13$ *TeV*, Eur. Phys. J. C **76** (2016) 292, arXiv: 1603.05598 [hep-ex].

[72] ATLAS Collaboration, *Expected performance of missing transverse momentum reconstruction for the ATLAS detector at* $\sqrt{s} = 13$ *TeV*, ATL-PHYS-PUB-2015-023, 2015, URL: https://cds.cern.ch/record/2037700.

[73] ATLAS Collaboration, *Performance of missing transverse momentum reconstruction with the ATLAS detector in the first proton–proton collisions at* $\sqrt{s} = 13$ *TeV*, ATL-PHYS-PUB-2015-027, 2015, URL: https://cds.cern.ch/record/2037904.

[74] C. G. Lester and D. J. Summers, *Measuring masses of semi-invisibly decaying particles pair produced at hadron colliders*, Phys. Lett. B **463** (1999) 99, arXiv: hep-ph/9906349 [hep-ph].

[75] A. Barr, C. Lester, and P. Stephens, *A variable for measuring masses at hadron colliders when missing energy is expected; m_{T2}: the truth behind the glamour*, J. Phys. G **29** (2003) 2343, arXiv: hep-ph/0304226.

[76] C. G. Lester and B. Nachman, *Bisection-based asymmetric M_{T2} computation: a higher precision calculator than existing symmetric methods*, JHEP **03** (2015) 100, arXiv: 1411.4312 [hep-ph].

[77] R. D. Cousins, J. T. Linnemann, and J. Tucker, *Evaluation of three methods for calculating statistical significance when incorporating a systematic uncertainty into a test of the background-only hypothesis for a Poisson process*, Nucl. Instrum. Meth. A **595** (2008) 480, arXiv: physics/0702156.

[78] R. D. Cousins, K. E. Hymes, and J. Tucker, *Frequentist evaluation of intervals estimated for a binomial parameter and for the ratio of Poisson means*, Nucl. Instrum. Meth. A **612** (2010) 388 , arXiv: 0905.3831.

[79] ATLAS Collaboration, *Multi-boson simulation for* 13 *TeV ATLAS analyses*, ATL-PHYS-PUB-2016-002, 2016, URL: https://cds.cern.ch/record/2119986.

[80] ATLAS Collaboration, *Monte Carlo Generators for the Production of a W or Z/γ^* Boson in Association with Jets at ATLAS in Run 2*, ATL-PHYS-PUB-2016-003, 2016, URL: https://cds.cern.ch/record/2120133.

[81] ATLAS Collaboration, *ATLAS simulation of boson plus jets processes in Run 2*, ATL-PHYS-PUB-2017-006, 2017, URL: https://cds.cern.ch/record/2261937.

[82] ATLAS Collaboration, *Modelling of the $t\bar{t}H$ and $t\bar{t}V$ ($V = W, Z$) processes for* $\sqrt{s} = 13$ *TeV ATLAS analyses*, ATL-PHYS-PUB-2016-005, 2016, URL: https://cds.cern.ch/record/2120826.

[83] M. Aliev et al., *HATHOR: HAdronic Top and Heavy quarks crOss section calculatoR*, Comput. Phys. Commun. **182** (2011) 1034, arXiv: 1007.1327 [hep-ph].

[84] P. Kant et al., *HatHor for single top-quark production: Updated predictions and uncertainty estimates for single top-quark production in hadronic collisions*, Comput. Phys. Commun. **191** (2015) 74, arXiv: 1406.4403 [hep-ph].

[85] N. Kidonakis, *Two-loop soft anomalous dimensions for single top quark associated production with a W^- or H^-*, Phys. Rev. **D82** (2010) 054018, arXiv: 1005.4451 [hep-ph].

[86] N. Kidonakis, "Top Quark Production," *Proceedings, Helmholtz International Summer School on Physics of Heavy Quarks and Hadrons (HQ 2013): JINR, Dubna, Russia, July 15-28, 2013*, 2014 139, arXiv: 1311.0283 [hep-ph].

[87] ATLAS Collaboration, *Jet Calibration and Systematic Uncertainties for Jets Reconstructed in the ATLAS Detector at $\sqrt{s}$ = 13 TeV*, ATL-PHYS-PUB-2015-015, 2015, URL: https://cds.cern.ch/record/2037613.

[88] ATLAS Collaboration, *Simulation of top-quark production for the ATLAS experiment at $\sqrt{s}$ = 13 TeV*, ATL-PHYS-PUB-2016-004, 2016, URL: https://cds.cern.ch/record/2120417.

[89] S. Frixione, E. Laenen, P. Motylinski, B. R. Webber, and C. D. White, *Single-top hadroproduction in association with a W boson*, JHEP **07** (2008) 029, arXiv: 0805.3067 [hep-ph].

[90] C. Borschensky et al., *Squark and gluino production cross sections in pp collisions at $\sqrt{s}$ = 13, 14, 33 and 100 TeV*, Eur. Phys. J. C **74** (2014) 3174, arXiv: 1407.5066 [hep-ph].

[91] M. Baak et al., *HistFitter software framework for statistical data analysis*, Eur. Phys. J. C **75** (2015) 153, arXiv: 1410.1280 [hep-ex].

[92] G. Cowan, K. Cranmer, E. Gross, and O. Vitells, *Asymptotic formulae for likelihood-based tests of new physics*, Eur. Phys. J. C **71** (2011) 1554, arXiv: 1007.1727 [physics.data-an], Erratum: Eur. Phys. J. C **73** (2013) 2501.

[93] A. L. Read, *Presentation of search results: the CL_s technique*, J. Phys. G **28** (2002) 2693.